



Vivaldi End-Fire Antenna for THz Photomixers

Mohammad Faraz Abdullah^{1,2} · Amlan K. Mukherjee² · Rajesh Kumar¹  · Sascha Preu²

Received: 13 November 2019 / Accepted: 6 February 2020 / Published online: 16 March 2020
© The Author(s) 2020

Abstract

We propose a broadband end-fire antenna for continuous-wave terahertz (THz) photomixing-based devices working in the frequency range of 0.5–1 THz. A compact Vivaldi antenna is presented that does not require any hyper-hemispherical silicon lens to collect and collimate THz radiation unlike the conventionally used broadside antennas. The antenna is tailored to radiate THz into or receive radiation from a dielectric waveguide placed in close vicinity of it. The antenna is fabricated on an indium phosphide (InP) substrate. A silicon (Si) superstrate is used to improve the directionality of the radiated beam. THz power coupled into Si waveguides is measured using two different techniques between 0.1 and 1.15 THz. Firstly, the waveguide is placed in the optical path of a 1550 nm based continuous-wave THz setup with a commercial broadside emitter, focusing optics, and a detector fabricated on the InP substrate with log-periodic broadside antenna. Secondly, the waveguide is placed in direct contact with the designed Vivaldi antenna-based THz receiver and using the commercial broadside emitter as a source. It is observed that the direct coupling technique using the Vivaldi end-fire antenna outperforms the optically coupled approach at frequencies higher than 668 GHz. Efficient THz photoconductive sources and receivers based on the designed compact Vivaldi end-fire antenna will be suitable for launching THz power into on-chip THz circuitry and for compact THz systems.

Keywords Photomixing · End-fire antenna · Terahertz · Continuous wave · Vivaldi antenna

✉ Rajesh Kumar
rajeshfph@iitr.ac.in

✉ Sascha Preu
preu@imp.tu-darmstadt.de

Amlan K. Mukherjee
mukherjee@imp.tu-darmstadt.de

¹ Department of Physics, Indian Institute of Technology Roorkee, Roorkee, India

² Department of Electrical Engineering and Information Technology, TU Darmstadt, Darmstadt, Germany

1 Introduction

Terahertz (THz, 0.1 to 10 THz) technology is becoming competitive to existing technologies in various areas like biology, spectroscopy, security, and communication [1–6]. The most widely used method to generate THz radiation with a bandwidth of several octaves is photomixing [6–9]. For continuous-wave generation, it involves mixing of two laser beams that are separated by the desired THz frequency in a photoconductive material in order to generate charge carriers with the beat frequency [6–10]. The generated charge carriers are collected at the electrodes by applying an external DC bias field or by a built-in internal field and subsequently fed into an antenna. In many cases, these are designed as planar broadside antennas (Fig. 1a)

like spiral- or logarithmic-periodic antennas. A hyper-hemispherical silicon lens, attached to the highly resistive substrate, usually assists outcoupling the THz power to free space. Furthermore, large optical components like parabolic mirrors (PMs) and plastic lenses are used for feeding into or outcoupling from waveguides. This optical coupling scheme is very bulky and the coupling efficiency may be poor depending on the waveguide, due to a mismatch of spot size and the mode field diameter of the waveguide.

Since the last decade, many researchers devised different techniques to improve the coupling between THz sources and various types of waveguides. For metallic wires with Sommerfeld waves, Deibel et al. enhanced the input coupling efficiency using a novel radially symmetric photoconductive antenna [11]. They end-coupled a radially polarized THz wave from the photoconductive antenna to metallic wire waveguide of cylindrical symmetry. To further improve the coupling, Zheng et al. optically coupled a polarization-controlled beam, generated by a segmented half-wave plate mode converter, to the bare copper wires using a THz lens [12]; however, the approach is narrow band. Recently, Hosseininejad et al. have presented an

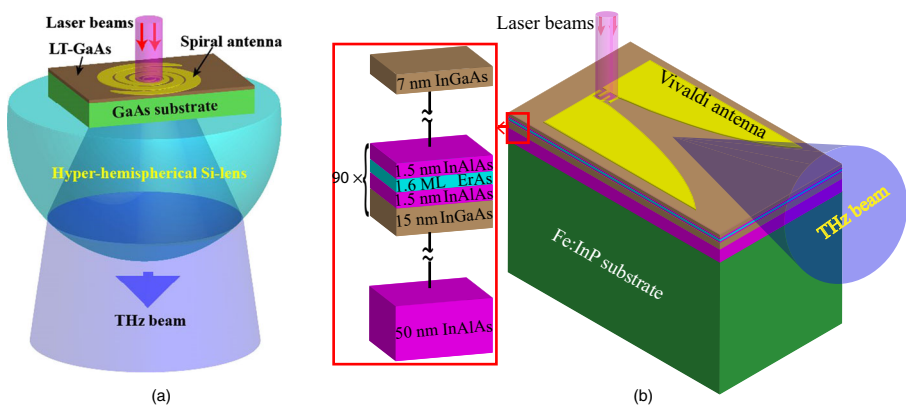


Fig. 1 a Conventional broadside emitting photoconductive antenna for operation with 800-nm lasers. b Photoconductive source for operation with telecom lasers attached to a Vivaldi end-fire antenna. The layers of the active material are shown in the inset

efficient approach for an exciting dielectric resonator antenna (DRA) in the THz frequencies using a graphene plasmonic dipole. They have attained improved efficiency [13] at resonance, i.e. in a narrowband configuration. Diwa et al. [14] designed and fabricated an integrated optics in the THz regime referring it as a “THz pigtail”. They experimentally proved the effectiveness of the fabricated lens duct in channeling and focusing the THz radiation from the emitter to the waveguide. Simplification of photomixers by removal of widely used Si-lens at the back side of the substrate is frequently addressed to make them more compact. Further, while semiconductor-based photomixers can be generally inexpensive once produced in large quantities, the Si-lens will remain a major cost factor. Rivera-Lavado et al. proposed a dielectric rod waveguide antenna at the backside of substrate as an alternative to the hyper-hemispherical Si-lens for THz photomixing devices. The waveguide antenna is cost-effective and avoids power scattering in the substrate [15]. Holdengreber et al. presented another antenna system based on a Josephson junction as a detecting element for 0.20-THz detection [16, 17]. They demonstrated high sensitivity detection without coupling lenses [16]. A significant work has been done in the direction of improving coupling between the THz sources and waveguides but still progressively increasing THz applications [1–5], and THz components, like planar dielectric waveguides, demand further improvement.

Our motivation is to design an end-fire antenna with the ability to couple the emitted THz radiation from a photomixer directly to a dielectric waveguide in a broadband fashion while avoiding bulky optics. We have chosen a Vivaldi antenna introduced by Gibson in 1988 [18]. The design is illustrated in Fig. 1b. It is a planar, travelling wave antenna having an exponentially tapered slot-line which may be impedance-matched over a wide bandwidth. These antennas are simple in geometry, easy to fabricate, and efficient. They offer wide bandwidth, significant gain, and symmetric radiation patterns. The Vivaldi antenna, hence, seems to be a good choice for this purpose. The reciprocity of the designed antenna facilitates the use of the antenna-coupled device both as a transmitter and receiver, the latter case being investigated in this paper.

2 Design and Simulations

The structure is similar to that shown in Fig. 1b. The Vivaldi antenna has an exponential taper that starts with a uniform slot-line and gradually flares out to a width around $\lambda_{\text{eff}}/2$. The radiation mechanism is based on the principle that the electric field is gradually transformed from a slot-line mode to a radiative mode by an exponential taper. The field is finally radiated when the distance between the two antenna arms reaches $\approx \lambda_{\text{eff}}/2$. Hence the highest and lowest frequency limits are defined by the slot width of the antenna at the feeding and radiating sections respectively. The beam pattern can be affected by its size, shape (length and taper), and material of the substrate (electric permittivity) [19]. The Ti/Au (10 nm/100 nm) antenna is shown in Fig. 1b in yellow, the substrate (green) modelled as InP with relative electric permittivity (ϵ_r) of 12.5 and loss tangent 0.0003. The Vivaldi antenna is modelled and optimized to get the desired polarization and a single mode, directive beam pattern.

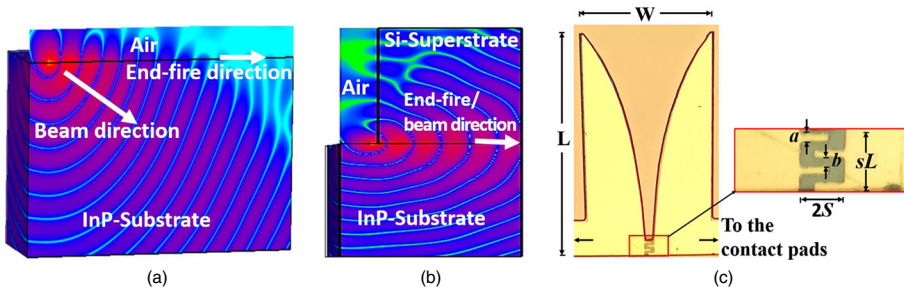


Fig. 2 The lateral cross section of the structure showing the E-field flow through the structure before **a** and after **b** attachment of the silicon superstrate. **c** Microscope image of fabricated device and finger structure in inset

The upper cut-off wavelength is approximated by the criterion as $\lambda_{\text{eff}}^{\text{max}} \sim 2W$, where W is the maximum distance between the two antenna arms. The minimum operation wavelength is defined by the slot-line width ($2S \ll \lambda_{\text{eff}}^{\text{min}}$). In the presented case, S is limited to the size of the photoconductive device of $10\mu\text{m} \times 10\mu\text{m}$.

The low wave impedance of substrate ($377/\sqrt{\epsilon_r} = 107\Omega$) causes the beam to bend down into the substrate as shown in Fig. 2a. To resolve this problem, a silicon ($\epsilon_r = 11.9$) superstrate of nearly the same thickness and dielectric constant as the InP substrate is attached on top of the antenna as depicted in Fig. 2b. The superstrate does not cover the feeding area, i.e. the finger electrode (cf. Fig. 2c) structure of the photoconductor which has to be irradiated with the laser beams. The antenna dimensions are chosen according to the wavelength in silicon in order to cover the frequency range of 0.5–2 THz. The final design parameters are summarized in Table 1. The length and the taper rate [20] are optimized for the small divergence and straight beam. First, simulations are repeated at different lengths of the antenna. At an antenna length around $184\mu\text{m}$, all investigated frequencies are emitted with a directivity larger than 3.3 dB. Longer lengths result in penalties at intermediate frequencies; shorter antenna lengths result in less directivity for all simulated frequencies. Thereafter, for the chosen length, the taper rate is varied to see its effect on directivity.

Table 1 Optimized dimensions of the Vivaldi antenna

Notations	Dimensions	Size
L	Length of antenna	$184\mu\text{m}$
W	Opening width	$120\mu\text{m}$
S	Half slot width	$5\mu\text{m}$
sL	Uniform slot length	$10\mu\text{m}$
r	Taper rate	$0.014\mu\text{m}^{-1}$
L_{sb}	Substrate length	$284\mu\text{m}$
W_{sb}	Substrate width	$170\mu\text{m}$
t_{sb}	Substrate thickness	$350\mu\text{m}$

The taper rate starts to result in directivity penalties above a rate of $0.014/\mu\text{m}$ for frequencies between 0.5 and 1.5 THz while at 2 THz, smaller taper rates seem disadvantageous. As a compromise, we opted for a taper rate of $0.014/\mu\text{m}$.

The simulation and optimization of the designed antennas are done in CST Microwave Studio, and the time domain solver is used, with open boundary conditions. For simplicity, the reciprocity theorem is applied for the simulations; i.e., the radiation patterns are obtained by emulation of the photoconductor as a THz source by a discrete port while they are later implemented as receivers in the experiment. The beam pattern of the above-modelled antennas are simulated at 0.5 THz, 0.6 THz, and 1 THz. Figure 2b shows that the antenna radiates straight in end-fire direction. However, the directivity is still very low.

3 Fabrication

The sample consists of an ErAs:In(Al)GaAs superlattice structure with 90 periods of 15 nm i-InGaAs, 1.5 nm p-InAlAs, 1.6 monolayers (ML) of p- δ -doped ErAs, followed by 1.5 nm p-InAlAs, similar to that in [21] just with twice the amount of erbium. It is illustrated in Fig. 1b. The substrate is semi-insulating Fe:InP. Standard processes consisting of UV photolithographical patterning of a photoresist, thermal metal evaporation Ti/Au (10 nm/100 nm), and photoresist-metal lift-off are used to define the biasing pads, finger structure, and the antenna and similarly for device definition. Finally, the finger structure region is coated with an anti-reflection coating (ARC) layer of silicon nitride.

The processed device is shown in Fig. 2c. The contacting pads of the antennas are bonded to a standard copper PCB with two traces using conductive epoxy and then the traces were soldered with a BNC (Bayonet Neill–Concelman) male connector to easily connect the device electrically. The device was mounted on a polyethylene (PE) holder using UV glue. The silicon superstrate was carefully aligned to the device, not covering the finger structure, and then fixed by UV glue.

4 Results and Discussion

The designed receiver photomixer with the Vivaldi antenna ($R_{x_{\text{viv}}}$) is characterized using a 1550 nm homodyne CW THz setup from TOPTICA photonics AG. A commercial InGaAs PIN photodiode ($T_{x_{\text{comm}}}$) from the Fraunhofer Heinrich Hertz Institute/TOPTICA Photonics AG is used as a THz transmitter [22]. It emits horizontally polarized THz waves. The difference frequency of the lasers can be tuned between 0 GHz and 2.75 THz [23]. The transmitter is bias-modulated between -1.5 and 0.5 V at 12 kHz which, in turn, modulates the THz signal. A photodetector fabricated from the same InP substrate as the $R_{x_{\text{viv}}}$ with a log-periodic antenna attached to a Si-Lens is used as reference receiver ($R_{x_{\text{ref}}}$), processed in the same processing run in order to minimize errors due to variations in the photoconductor material properties and the processing. The receiver detects amplitude and phase of the radiated E-field from the transmitter. A PDA-S low noise transimpedance amplifier from

TEM Messtechnik with a transimpedance of 10^6 V/A, amplifies the detected photocurrent prior to lock-in detection.

First, in Fig. 3, we compare the dynamic range of the designed Rx_{viv} with Rx_{ref} within a free space setup. As the beam patterns of the Vivaldi antenna and the reference device are quite different, the optical setups for both measurements were different. For the reference measurement, a well-known, close to optimum beam propagation configuration was used. It consisted of Tx_{comm} that emits a divergent beam with a focal point roughly 1 cm behind the device. A parabolic reflector, aligned to this focal point collimates the beam. Two TPX lenses generate an intermediate focus and then collimate the beam again. Finally, a parabolic mirror images the beam on the reference receiver Rx_{ref} . For measuring Rx_{viv} , unfortunately, no optimum beam propagation with ordinary lens optics exists. The best results were achieved with a setup consisting of Tx_{comm} , followed by a parabolic mirror that generates a collimated beam and a TPX lens that focuses the beam on the tip of the Vivaldi antenna. The dynamic range of the end-fire receiver is observed to be approximately 30 dB lower than that of the reference receiver over the whole measurement range. The material-dependent roll-off characteristics are similar in both Rx_{viv} and Rx_{ref} . The lower dynamic range can be attributed to inadequate beam propagation from source to receiver and the absence of a prefocusing Si-lens in the case of Rx_{viv} that assists in incoupling for the case of the reference receiver. The results for the reference receiver with a logarithmic-periodic antenna but without the Si-lens are obtained the same way and presented in the same figure. For emission into free space, the reference antenna without Si-lens and the end-fire antenna show comparable performance except for frequencies below 300 GHz where the reference antenna is slightly better. This is in line with the fact that the Vivaldi antenna is designed only for frequencies

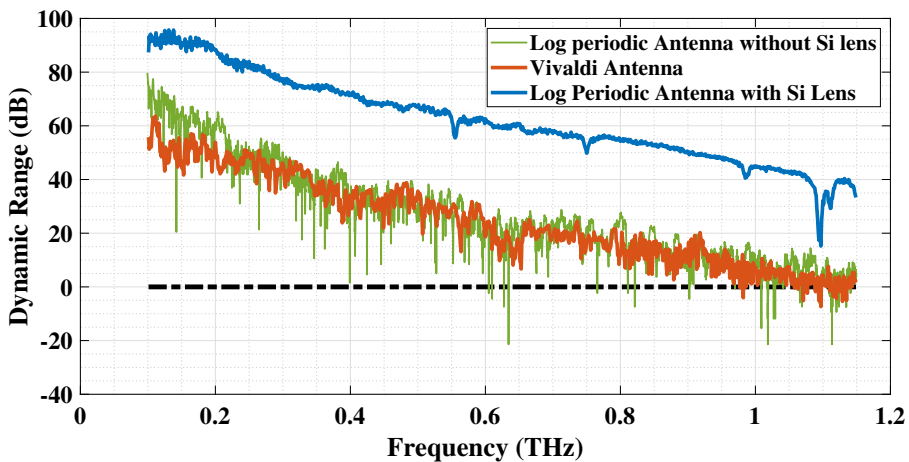


Fig. 3 A comparison between the measured dynamic ranges of setups as described in text with Rx_{ref} and Rx_{viv} as receivers. For the reference measurement, a beam propagation setup was used that is known as close to ideal for the radiation patterns of the broadside emitting device Rx_{ref} . For the Vivaldi antenna, the beam is just partially captured by the used optics

above 500 GHz. This performance along with end-fire emission characteristic makes the proposed Vivaldi antenna suitable for integrated THz circuits.

Second, we study the emitted beam pattern of the Vivaldi antenna and compare it to the simulated results. Owing to the low dynamic range at higher frequencies (Fig. 3), 500 GHz and 600 GHz are selected for the beam pattern measurement. The beam pattern in the far-field is measured by two planar line scans in x and y direction by mounting the Tx_{comm} together with a lens on a 2D stage. The distance between receiver and lens is 11.5 cm, and between lens and transmitter is 2.5 cm. Care is taken that Tx_{comm} always points directly towards the center of Rx_{viv} . At each point, we perform frequency scans at 500 and 600 GHz and extract the field amplitude information. Finally, the planar far field data, E_{xy} , are transformed to the spherical plane for comparison with simulations by using

$$E_{xy} \propto \frac{1}{r} \quad (1)$$

Therefore,

$$E_{\text{arc}} = \frac{\sqrt{r^2 + x^2 + y^2}}{r} E_{xy} \quad (2)$$

and the corresponding angle

$$\phi = \arctan \left(\sqrt{\frac{x^2 + y^2}{r}} \right) \quad (3)$$

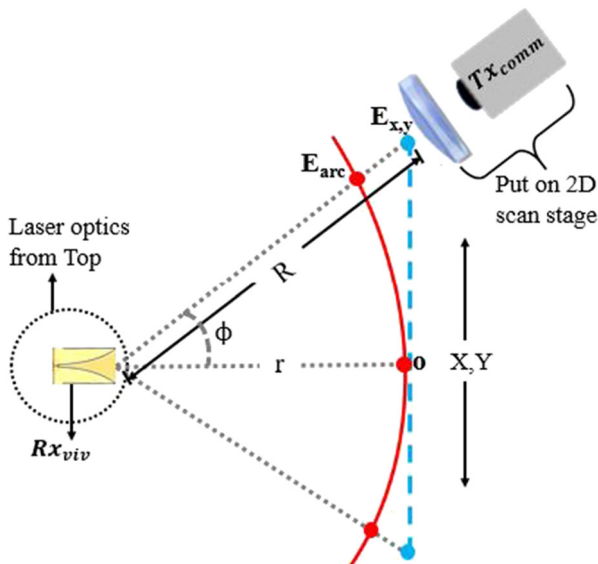


Fig. 4 Projection of the plane image (blued dashed line) to spherical geometry (red solid line) for obtaining E_{arc}

where E_{arc} is the projection of the field E_{xy} on a sphere with radius r which is the distance of the 2D plane to Rx_{viv} as illustrated in Fig. 4. The corrected E- and H-plane beam patterns for 500 GHz and 600 GHz are plotted in Fig. 5. There is an excellent agreement between experiment and simulations.

Finally, we investigate the power coupling efficiency to a high resistive float zone (HRFZ) silicon waveguide with a rectangular cross section of $280 \mu\text{m} \times 500 \mu\text{m}$ and a length of 50 mm, attached on top of a polyethylene (PE) substrate. First, we measure power received at Rx_{ref} using an optical coupling technique (P_{oc}): The emitted THz beam of the source Tx_{comm} is collimated with a protected silver 90° off-axis parabolic mirror and then focused on the waveguide aperture by a plano-convex aspherical TPX lens. The waveguide is bent by about $\sim 10^\circ$ to prevent line of sight coupling between the THz transmitter and receiver optics. When the waveguide is moved out of place, no detectable signal is observed in the receiver thus confirming negligible line of sight coupling. The guided wave exits the waveguide and is captured with another

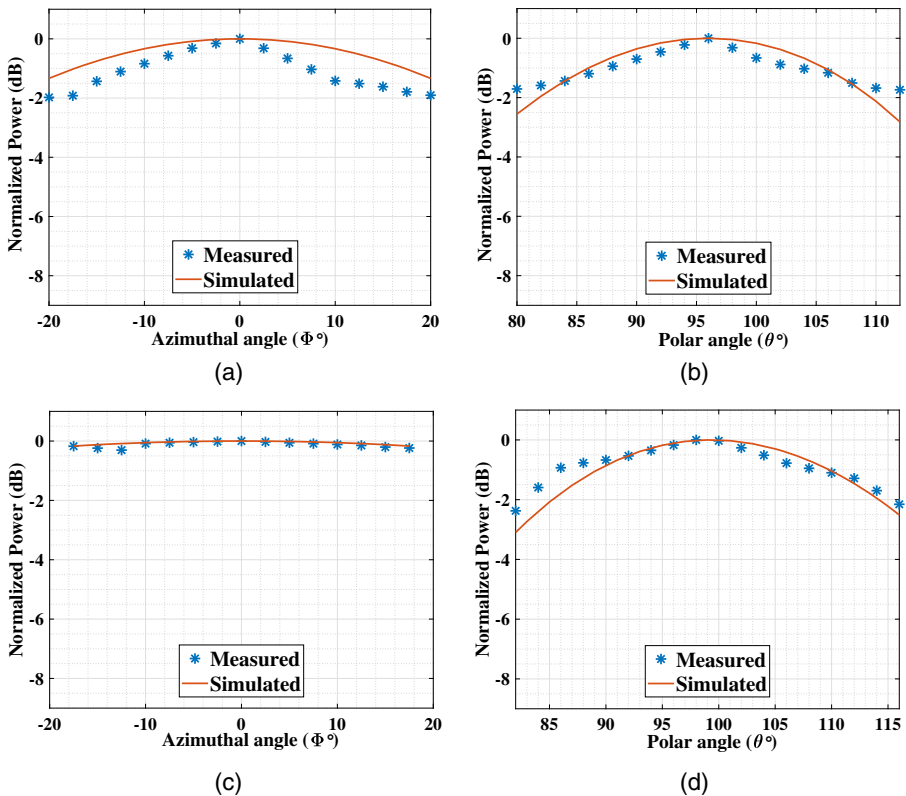


Fig. 5 Beam pattern plots at 500 GHz for E (a) and H planes (b), and at 600 GHz for E (c) and H planes (d)

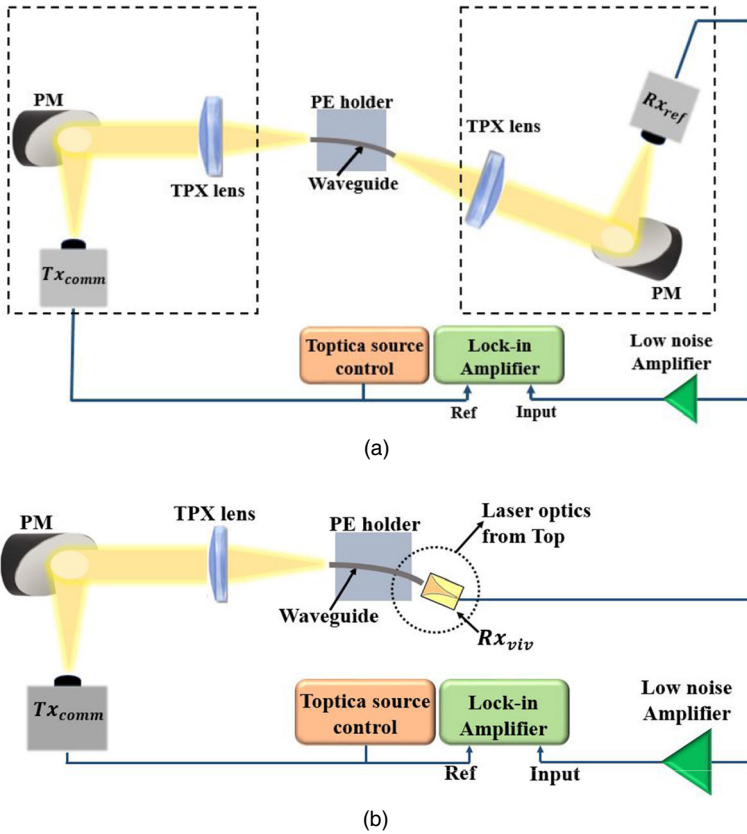


Fig. 6 Schematics of the experimental setup for **a** optical coupling and **b** direct coupling measurements

TPX lens prior to focusing on Rx_{ref} using another parabolic mirror as illustrated in Fig. 6a.

For direct coupling, the receiver side (right dashed box in Fig. 6a) is replaced by the Rx_{viv} and brought in physical contact with the waveguide as shown in Fig. 6b. A Si superstrate increases the effective refractive index of the antenna system resulting in worse matching to the propagating waveguide mode. Therefore, the Si superstrate is not used in this case. In order to compensate for the off-axis emission of the antenna without Si superstrate (c.f. Fig. 2a), the waveguide is vertically displaced with respect to the Rx_{viv} to maximize the coupled power. The power received at the Vivaldi receiver (P_{dc}) is measured and compared with the optically coupled power, P_{oc} , in Fig. 7, that shows the ratio of both. The power ratio is determined by the fact that a photoconductive THz receiver is a field detector and generates photocurrent proportional to the incident electric field. The received power at the receiver is pro-

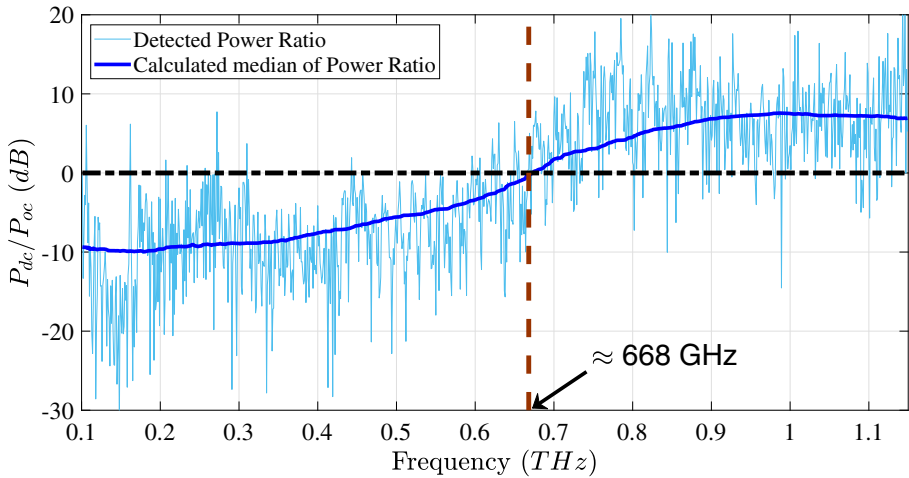


Fig. 7 Plot for the frequency vs. relative transmission coefficient for the Vivaldi $R_{x_{viv}}$. The large fluctuations in the plot originate from standing waves within the waveguide as well as in the minute gap between the waveguide and $R_{x_{viv}}$ and potentially the Vivaldi antenna substrate

portional to the squared value of the measured photocurrent with a proportionality constant, k . Thus, the power ratio (P_{dc}/P_{oc}) can be calculated as

$$\begin{aligned} \frac{P_{dc}}{P_{oc}} &= \frac{k \cdot I_{dc}^2}{k \cdot I_{oc}^2} \\ &= \left(\frac{I_{dc}}{I_{oc}} \right)^2 \end{aligned} \tag{4}$$

where I_{dc} and I_{oc} are the detected photocurrents in direct and optical coupling scenarios. The median line is drawn to show the trend of the detected power ratio. Figure 7 shows that above ≈ 668 GHz, the power ratio exceeds unity (0 dB); i.e. the coupling to the Vivaldi antenna is more efficient than the optical coupling technique. This proves that the design of the Vivaldi antenna is much more appropriate for waveguide coupling. Between 0.8 and 1 THz, the power detected by the Vivaldi antenna is four times (6 dB) higher than the power received by the optical coupling setup, which makes the end-fire antenna more suitable for coupling power into waveguides placed in vicinity. It also proves the effectiveness of the Vivaldi antenna: While the Si-lens-coupled logarithmic periodic antenna in Fig. 3 outperforms the Vivaldi antenna by 35 dB at 1 THz in free space, the Vivaldi antenna outperforms at waveguide coupling by 6 dB. Considering the fact that at each end of the waveguide a coupling structure is required, replacement of Si-lens-coupled antennas by Vivaldi end-fire antennas improves coupling by 9 dB. The frequency of ≈ 668 GHz at which the Vivaldi antenna exceeds the performance of the optical coupling setup also agrees fairly well with the lower cut-off frequency of the design of about 500 GHz.

5 Conclusion and Outlook

A Vivaldi end-fire antenna for direct coupling of radiation from a dielectric waveguide to a THz photoconductive source has been demonstrated. The beam patterns at frequencies 500 and 600 GHz agree well with simulations. Off-axis emission caused by the high index substrate was compensated by a silicon superstrate with almost identical refractive index. Simulations show that proper end-fire emission can also be achieved by substrate thinning to a thickness below few microns at a design frequency of 1 THz. The Vivaldi antenna, directly attached to a $280 \times 500 \mu\text{m}^2$ high resistivity silicon waveguide, outperforms collection of the THz power with the aid of a TPX lens and a parabolic mirror coupled to a broadside antenna with silicon lens within its design frequency range. This allows to omit bulky optics such as parabolic mirrors and TPX and silicon lenses and enables chip-size packaging of sources, detectors, and waveguides.

Acknowledgments We acknowledge Computer Simulation Technologies (CST) AG for the EM Simulation solver. We also thank Justin C. Norman and Arthur C. Gossard, both at the University of California, Santa Barbara, Santa Barbara, USA, for growth of the ErAs:InAlGaAs sample.

Funding Information This research is financially supported by the European Research Council (ERC) through the Starting Grant Pho-T-Lyze with project number 713780 (SP) and FIG Scheme of Indian Institute of Technology Roorkee (RK).

Open Access This article is licensed under a Creative Commons Attribution 4.0 International License, which permits use, sharing, adaptation, distribution and reproduction in any medium or format, as long as you give appropriate credit to the original author(s) and the source, provide a link to the Creative Commons licence, and indicate if changes were made. The images or other third party material in this article are included in the article's Creative Commons licence, unless indicated otherwise in a credit line to the material. If material is not included in the article's Creative Commons licence and your intended use is not permitted by statutory regulation or exceeds the permitted use, you will need to obtain permission directly from the copyright holder. To view a copy of this licence, visit <http://creativecommons.org/licenses/by/4.0/>.

References

1. P.H. Siegel, IEEE transactions on microwave theory and techniques **52**(10), 2438 (2004).
2. P.U. Jepsen, D.G. Cooke, M. Koch, Laser & Photonics Reviews **5**(1), 124 (2011).
3. J.F. Federici, B. Schulkin, F. Huang, D. Gary, R. Barat, F. Oliveira, D. Zimdars, Semiconductor Science and Technology **20**(7), S266 (2005).
4. R. Dickie, R. Cahill, V. Fusco, H.S. Gamble, N. Mitchell, IEEE Transactions on Terahertz Science and Technology **1**(2), 450 (2011).
5. T. Nagatsuma, G. Ducournau, C.C. Renaud, Nature Photonics **10**(6), 371 (2016).
6. S. Preu, G. Döhler, S. Malzer, L. Wang, A. Gossard, Journal of Applied Physics **109**(6), 4 (2011).
7. A. D.J. Fernandez Olvera, H. Lu, A. C. Gossard, S. Preu, Optics Express **25**(23), 29492 (2017).
8. D. Saeedkia, S. Safavi-Naeini, IEEE photonics technology letters **18**(13), 1457 (2006).
9. D. Saeedkia, R.R. Mansour, S. Safavi-Naeini, IEEE transactions on applied superconductivity **15**(3), 3847 (2005).
10. M. Tani, O. Morikawa, S. Matsuura, M. Hangyo, Semiconductor Science and Technology **20**(7), S151 (2005).
11. J.A. Deibel, K. Wang, M.D. Escarra, D.M. Mittleman, Optics express **14**(1), 279 (2006).

12. Z. Zheng, N. Kanda, K. Konishi, M. Kuwata-Gonokami, in: *The European Conference on Lasers and Electro-Optics* (Optical Society of America, 2013), p. CC.P_7.
13. S.E. Hosseinijad, M. Neshat, R. Faraji-Dana, S. Abadal, M.C. Lemme, P.H. Bolivar, E. Alarcón, A. Cabellos-Aparicio.(2018).
14. G. Diwa, A. Quema, E. Estacio, H. Murakami, S. Ono, N. Sarukura, in: *2005 Joint 30th International Conference on Infrared and Millimeter Waves and 13th International Conference on Terahertz Electronics*, vol. 1 (IEEE, 2005), vol. 1, pp. 283–284.
15. A. Rivera-Lavado, S. Preu, L.E. García-Muñoz, A. Generalov, J. Montero-de Paz, G. Döhler, D. Lioubtchenko, M. Méndez-Aller, F. Sedlmeir, M. Schneidereit, et al., *IEEE Transactions on Antennas and Propagation* **63**(3), 882 (2015).
16. E. Holdengreber, A. Moshe, M. Mizrahi, V. Khavkin, S. Schacham, E. Farber, *Journal of Electromagnetic Waves and Applications* **33**(2), 193 (2019).
17. E. Holdengreber, X. Gao, M. Mizrahi, S. Schacham, E. Farber, *Superconductor Science and Technology* **32**(7), 074006 (2019).
18. P. Gibson, in: *1979 9th European Microwave Conference* (IEEE, 1979), pp. 101–105.
19. P. Ludlow, V. Fusco, in: *2009 Loughborough Antennas & Propagation Conference* (IEEE, 2009), pp. 445–448.
20. C.A. Balanis, *Antenna theory: analysis and design* (John wiley & sons, 2016), pp. 497–498.
21. D. Driscoll, M. Hanson, A. Gossard, E. Brown, *Applied Physics Letters* **86**(5), 051908 (2005).
22. <https://www.toptica.com/products/terahertz-systems/frequency-domain/gaas-and-ingaas-photomixers/>. Accessed:10-09-2019.
23. A.J. Deninger, A. Roggenbuck, S. Schindler, S. Preu, *Journal of Infrared, Millimeter, and Terahertz Waves* **36**(3), 269 (2015).

Publisher's Note Springer Nature remains neutral with regard to jurisdictional claims in published maps and institutional affiliations.